Neurobiology of Stress 29 (2024) 100601

Contents lists available at ScienceDirect

Neurobiology of Stress

journal homepage: www.elsevier.com/locate/ynstr

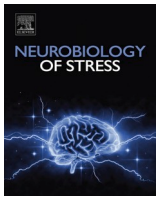

An epigenetic mechanism of social isolation stress in adolescent female mice

Pei Li, Zhen Yan *

Department of Physiology and Biophysics, Jacobs School of Medicine and Biomedical Sciences, State University of New York at Buffalo, Buffalo, NY, 14203, USA

ARTICLE INFO

Keywords:
Isolation stress
Female
Anxiety
Epigenetics
Histone methylation
Arc

ABSTRACT

Social isolation during adolescence can increase the risk of mental disorders. Epigenetic changes induced by chronic social isolation may serve as a mechanism underlying emotional disturbances. To test this, we exposed female mice to a post-weaning 6-week social isolation (SI) stress. We found the significantly increased methylation of histone H3 at lysine 9 (H3K9), a histone mark linked to gene repression, as well as the increased H3K9 methyltransferases SUV39H1 and SETDB1, in prefrontal cortex (PFC) of SI females. To find out potential downstream genes affected by this epigenetic alteration, we examined genes linked to neuronal and synaptic functions. Activity-dependent genes, including *Arc, c-Fos and Npas4,* were significantly reduced in PFC of SI females, correlated with the increased H3K9me2 occupancy around *Arc* enhancer. Treatment of SI females with UNC0642, a selective inhibitor of H3K9 methylation, significantly attenuated the anxiety-like behavior and elevated *Arc* expression. These results have revealed an epigenetic mechanism and intervention avenue for anxiety induced by chronic social isolation.

1. Introduction

Emerging evidence suggests that chronic lack of social contacts during adolescence has a negative effect on mental and physical health (Lee et al., 2021; Loades et al., 2020; Snyder-Mackler et al., 2020). The adolescence is critical for brain maturation and behavioral development and peer interactions become progressively important during this period (Woodhouse et al., 2012). Prolonged isolation during adolescence has been linked to anxiety, hyperactivity, social problem, and aggression, along with widespread structural and functional changes in the brain (Sun et al., 2017; Tan et al., 2021; Wang et al., 2022b; Zelikowsky et al., 2018).

Epigenetic dysregulation of gene expression is identified as an important mechanism underlying a variety of brain disorders (Cao et al., 2020; Qin et al., 2021; Sanacora et al., 2022; Tran et al., 2015). Different kinds of stress can induce the alteration of histone modifications (Kundakovic et al., 2013; Stankiewicz et al., 2013; Suri et al., 2013), the processes carried out by a group of enzymes via adding or removing specific chemical groups on histone proteins, which can lead to the activation or repression of gene transcription. Social isolation stress in adult male mice was found to cause epigenetic changes in midbrain, including increased methylation of H3 lysine 4 and acetylation of H3 lysine 9 (both linked to gene activation), as well as the enhanced histone methyltransferases and histone deacetylases (Siuda et al., 2014). Targeting epigenetic enzymes to normalize gene expression has been reported to mitigate behavioral defects in various brain diseases, such as Alzheimer disease and autism (Cao et al., 2020; Wang et al., 2022a; Zheng et al., 2019).

Prefrontal cortex (PFC), which is comprised of prelimbic (PL), infralimbic (IL) and anterior cingulate cortex (ACC), is a key brain region controlling high-level cognitive and emotional processes (Carlén, 2017; Franklin et al., 2017; Reinert et al., 2021). Dysfunction of PFC and its dysregulation of interconnected target areas have been implicated in many neuropsychiatric diseases, including anxiety and depression (Hare and Duman, 2020; Kim and Whalen, 2009; Shackman et al., 2011; Yan and Rein, 2022). Our previous studies have found the decreased neuronal activity in PFC of SI mice (Tan et al., 2021; Wang et al., 2022b). In the current study, we sought to find out whether chronic adolescent social isolation induces epigenetic alterations in PFC, leading to manifestation of behavioral abnormalities, and whether epigenetic-based treatment is a viable intervention strategy.

* Corresponding author.
E-mail address: zhenyan@buffalo.edu (Z. Yan).

https://doi.org/10.1016/j.ynstr.2023.100601
Received 11 September 2023; Received in revised form 1 December 2023; Accepted 11 December 2023
Available online 18 December 2023

2. Materials and methods

2.1. Animals and chemicals

All experiments were performed with the approval of the institutional animal care and use committee (IACUC) in State University of New York at Buffalo. Chronic social isolation was modified from our previous work (Wang et al., 2022b). Female C57BL/6J mice (Strain#: 000664) were socially isolated for 6 weeks from weaning (postnatal day 21) to postnatal day 63, which covered the whole adolescence (Tirelli et al., 2003). Mice were randomly divided into the group-housed (GH) or socially-isolated (SI) group. Each GH cage has 2–4 mice, bedding and enrichment (paper strips for nesting and a paper roll for hiding and playing), while each SI cage has 1 mouse, bedding, and nesting materials. SI cages were also covered with opaque plastic film to avoid visual communication with outside social stimuli. All animals were housed with ad libitum food accessibility in 12h light/dark cycle (light: 7 a.m.-7 pm).

UNC0642 (Tocris, 5132), GSK126 (Tocris, 6790/5), or Romidepsin (Selleckchem, S3020) was dissolved in Dimethyl sulfoxide (DMSO, Sigma-Aldrich, D2650) to make the stock solution and stored at −20 °C. Before use, stock solution was diluted with saline, so DMSO concentration was lower than 1%. Behavior tests were carried out 24 h after the last drug administration, followed by tissue collection.

2.2. Behavior tests

All behavior tests were conducted in dim light and carried out between 10 a.m. and 6 p.m. Mice were transferred to the test room for at least 1 h before behavioral assays. Apparatus was cleaned with 70% ethanol to avoid interfering between different animals. Any-maze software was used to track, record and measure. Mice were sacrificed 24 h after behavioral experiments for tissue collection and *in vitro* experiments.

Elevated plus maze (EPM) test was performed as previously described with minor changes (Walf and Frye, 2007; Wang et al., 2022b). The plus shaped EPM (48 cm off the floor) consists of two open arms (length, 40 cm; width, 7.5 cm) and two closed arms (length, 40 cm; width, 7.5 cm; height, 27.5 cm; with black walls). Mice were placed in the center area of EPM and headed to the same open arm. The time in open or closed arms, the number of entries to open or closed arms, the latency to open arms, and total distance traveled were recorded during the 10-min test. Because repeated EPM tests significantly affected mouse behaviors, all the results represented independent experiments, and no mice were repeatedly used.

Open field (OF) test was used to assess the locomotor activity. Mice were placed in an arena (length and width, 48 cm; height, 38 cm). Total distance and the time spent in the center area (length and width, 24 cm) were recorded during the 10-min test.

Barnes maze (BM) test was used to measure spatial memory as previously described (Cao et al., 2020). Three different images on the surrounding walls were used as visual cues. Briefly, the mouse was placed on a round platform (diameter, 90 cm; height, 24 cm) with evenly spaced 8 holes (diameter, 5 cm) located 2.5 cm away from the edge. One of the holes (correct) had an attached escape box. The platform was brightly lit, serving as an aversive stimulus. The mouse was trained twice (5-min each, 5-min interval) until it entered the escape box. Then it was allowed to rest for 15 min at the home cage. Next, the mouse was placed back on the platform (escape box removed). The time spent around the correct hole (T1) and the other 7 incorrect holes (T2) were recorded during the 5-min test. The spatial memory index was calculated as T1/T2.

2.3. Quantitative real-time RT-PCR

Mouse PFC (PL, IL, and ACC) was dissected based on the location from Bregma (AP: 1.34–2.96 mm, ML: ±0.75 mm, DV: 0–3 mm). Total RNA was isolated using Trizol reagent (Invitrogen, 15596026). iScriptTM cDNA synthesis Kit (Bio-Rad, 1708891) was used to obtain cDNA from the tissue mRNA. Quantitative real-time PCR was carried out using the CFX Connect Real-Time PCR Detection System and iQ™ SYBR® Green Supermix (Bio-Rad, 1708882). GAPDH was used as the housekeeping gene for quantitation of the expression of target genes. A total reaction mixture of 20 μl was amplified in a 96-well thin-well PCR plate (Bio-Rad, HSP9601) using the following PCR cycling parameters: 95 °C for 3 min followed by 40 cycles of 95 °C for 15 s, 60 °C for 20 s, and 72 °C for 30 s. Fold changes in the target genes were calculated as following: ΔCt = Ct(target) – Ct(GAPDH), and Δ(ΔCt) = ΔCt(SI) – mean ΔCt(GH) or Δ(ΔCt) = ΔCt (SI + drug)− mean ΔCt(SI + DMSO), and Fold change = $2^{-\Delta(\Delta Ct)}$. The list of primers used in qPCR experiments is as follows.

Mouse Target Gene	Forward	Reverse
Ehmt1	GGCACTGATGTCAGGGTTCA	GCTGTCTGGGACTTTGTGGT
Ehmt2	GCTCCACCTGTCTACATCAT	GCAGATGTTTTCCTCATTGT
Setdb1	ACCCGTCCTAATATGGGTGCT	AGCTTTCAGTGTCAGCTGCTT
Suv39h1	AACATGCAAGTGGACCCCG	GGTATTTTCGGCAAGCCGTT
Suv39h2	TTCACAGTGGATGCAGCTCG	TGCTTCTCCAGAACCTTTCATT
Kdm4d	GATTTGGAGCGAAAATACTG	ACTATGCCACATTCCTGTTC
Setd1a	TGTGCTCTTCACCAGCACTC	CAGTGGGCACAGTCTGAGG
Setd1b	GCGAGAGGAGGAACCACCAT	ACAGCTCCAGCTCCTTGTTTTT
Kmt2a	AAAAGCAACAGGGCGGAAGA	TGGCAACCCTCTTGTCAGTC
Kmt2d	GGTGCAGCAGAAGATGGTGA	GTCTGATTGTGAGGGGGTGT
Kdm5d	CTAAATGAACTGGAGGCCC	ACGGTCCTTGCAGATTGCTT
Hdac2	ATGGCGTACAGTCAAGGAG	CCATTTTTCGGTATAAACCAT
Hdac3	ATCATGCCAAGAAATTTGAG	AGGTAGAAGGCTTCCTGAAC
Ep300	GTGAACAACATGAGTGCTAGTCC	GCCACACCAGCATTTTCACT
Chd4	GAAATTGCTGCGGCACCATTA	AGCCATCATTGTAGTTGACCTG
Chd5	GAACATGAACGAGTACCTGAGC	GTAGTTGACCTGCTTGCGGAT
Arid1a	GTCTTCCACCAACAACATGG	AGGAGTTGTACTGGTGGTTG
Stat3	ACTTCAGACCCGCCAACAAA	CACCACGAAGGCACTCTTCA
Rest	CAGCACGTGCGAACTCACAG	CTCACCTGAATGAGTCCGCATGTGTC
Ncor2	CCTCTGGAAGCAGCAGCC	GCTGCGAGGTGATGTAGTCA
Npas4	ACCTAGCCCTACTGGACGTT	CTTTCAGCCAACAGGCGGTA
Arc	GAACCTCAACTTCCGGGGAT	ACTGGTATGAATCACTGGGGG
c-Fos	GGGAATGGTGAAGACCGTGTCA	GCAGCCATCTTATTCCGTTCCC
Egr1	GAATCTGCATGCGTAACTTC	GATTTTGGTATGCCTCTTGC

(*continued on next page*)

(*continued*)

Mouse Target Gene	Forward	Reverse
Bdnf	GGGGCATAGACAAAAGGCAC	AATGGTCAGTGTACATACACAGGAA
Ntrk2	CCACGGATGTTGCTGACCAAAG	GCCAAACTTGGAATGTCTCGCC
Nrxn1	GCCCCAGTACACGAGCAG	GCGATGTCATCTGTCCCAAC
Stx6	AGCTGAGGAACAATCTCCGC	TCTGATCCTTCATGTCCCTGAC
Synaptotagmin-1 (Syt1)	TGAAACTGGACTGACTGATG	CAGCTGGTTATTCTGGAAGT
Synapsin 1 (Syn1)	AAGTTCTTCGGAATGGAGTC	ATGACCAAACTTCGGTAGTC
Synaptophysin (Syp)	CCTAGTTGGTGACTACTCCT	GTTGTTCTCTCGGTACTTGT
Syntaxin-1A (Stx1a)	GGACATTAAGAAGACAGCGA	ACATGACCTCCACAAACTTT
Snap25	GGATGAGCAAGGCGAACAAC	TGGCCACTACTCCATCCTGA
Dlg4	AGCCCCAGGATATGTGAACG	TCACCGATGTGTGGGTTGTC
Slc6a1	GGTAGTCAAGGTGCAGAAGA	AAGATGAGCGTCAGGAAATA
Slc6a11	CTGATTCCTTACGTGGTGTT	ATAGCCAATGCCTTCAAATA
Slc6a12	GAAGTGGCTGAGTCAGGTCC	CCAGCCCTAGAAACAGGAGC
Slc6a13	GCTGTGTGCCTGGCGA	GAGCTGGCGAAGTCTCTCTC
Gabra1	CACCATGAGGTTGACCGTGA	CTACAACCACTGAACGGGCT
Gabra2	GGTGTGGGACCCAGTCAGGT	GACAGGGCCAAAACTGGTCACG
Gabrb2	ATTTGGTGGCTCAAACGGTC	GAGATTTCCTCACCAGCAGGA
Gabrg2	GGAGCCGGCATCAAATCATC	CTTTTGGCTTGTGAAGCCTGG
Gabrd	ATACACCATGACTGTGTTCC	TAGGCGGATAAGCTTGTTTT
Pvalb	GGTGAAGAAGGTGTTCCATA	CAGACAAGTCTCTGGCATCT
Bassoon	CCAGAGAACAACTTCTCCAA	CTGTGTCCTGCTGTCTACCT
Grin1	CATCGGACTTCAGCTAATCA	GTCCCCATCCTCATTGAATT
Grin2a	GGCTACAGAGACTTCATCAG	ATCCAGAAGAAATCGTAGCC
Grin2b	TTAACAACTCCGTACCTGTG	TGGAACTTCTTGTCACTCAG
Grm2	GCTTAGGTTCCTGGCACT	TTAACAGGTCCACACTCCTC
Grm3	CAATTACTTGCTTCCAGGAG	TAGTCAACGATGCTCTGACA
Gria1	GCCTTAATCGAGTTCTGCTA	GAATGGATTGCATGGACTTG
Gria2	AGCCTATGAGATCTGGATGT	GAGAGAGATCTTGGCGAAAT
Shank3	GATCTGCCATCCCTACAAC	AGCTAAGGGTGAGCTAGGAT
Homer1a	GGCAAACACTGTTTATGGAC	GAGACTGAAGATCTCCTCCT
Ezh1	AAAGTCAACACTTCCCGCTG	CATACAGAGCCTTTGCTCCCA
Ezh2	TCCATGCAACACCCAACACA	CCTTAGCTCCCTCCAGATGC
Kdm6a	GCATTTCAGGAGGTGCTT	CATTGGACAAAGTGCAGGGA
Kdm6b	AGGAGTCACTGCAGGAGGAGAG	CCACCTCTTGGCATCAGACAG
Gapdh	GACAACTCACTCAAGATTGTCAG	ATGGCATGGACTGTGGTCATGAG

2.4. Western blotting for nuclear proteins

Nuclear extraction from mouse brain was performed as we described before (Qin et al., 2021) with modifications. Briefly, PFC was collected and homogenized with 250 μl hypotonic buffer (20 mM Tris-HCl, pH 7.4, 10 mM NaCl, and 3 mM $MgCl_2$) including protease inhibitor cocktail (1:50) and 1 mM PMSF. After incubation on ice for 15 min, the homogenate was added with 12.5 μl NP-40 (10%) and vortexed for 10 s. Then the homogenate was centrifuged at 3000 g, 4 °C for 10 min. The nuclear pellet was resuspended in filtered 1% SDS with protease inhibitor cocktail and 1 mM PMSF. Protein concentration was measured by Pierce™ BCA Protein Assay Kit (Thermo Scientific, 23227). All the samples were set to the same concentration and boiled with 4 x SDS loading buffer for 10 min. According to the size of the proteins, 12% SDS-polyacrylamide gels were used. Samples (5–15 μg) were loaded according to the sensitivity of different antibodies. Western blotting experiments for nuclear proteins were performed with antibodies against Histone 3 (cell signaling, 4499, 1:1000), H3K9me2 (cell signaling, 4658, 1:1000), and H3K9me3 (Invitrogen, PA5-31910, 1:1000). Blots were incubated with the HRP-conjugated second antibodies (1:2000) for 2–3 h at room temperature. SuperSignal™ West Pico PLUS Chemiluminescent Substrate (ThermoFisher Scientific, 34580) and super signal west Femto Maximum sensitivity substrate (ThermoFisher Scientific, 34095) were used to detect protein signals.

2.5. Immunostaining

Mice were anesthetized and transcardially perfused with phosphate buffered saline (PBS) and 4% fresh prepared paraformaldehyde (PFA) before brain removal (Qin et al., 2021). Brains were post-fixed in 4% PFA overnight, dehydrated in 30% sucrose for 2 days and cut into 50 μm PFC-containing slices coronally. After washing with PBS for 3 times (10 min each), slices were blocked in PBS containing 5% BSA and 0.3% Triton for 2 h at room temperature. Then slices were incubated with primary antibody against H3K9me3 (1:500, Invitrogen, PA5-31910), H3K4me3 (1:500; Cell Signaling, 9751), H3K27me3 (1:1000, Cell Signaling, 9733S) or NeuN (1:500; Millipore, MAB377) overnight at 4 °C. After washing with PBS for 3 times (15 min each), slices were incubated with secondary antibodies, Alexa Fluor 488 (1:1000; Invitrogen, A32723) and Alexa Fluor 546 (1:1000; Invitrogen, A11035), for 2 h at room temperature. DAPI (ThermoFisher, D1306, 5 μg/ml) was used to stain nucleus for 30 min at room temperature. ProLong™ Diamond Antifade Mountant (Invitrogen, P36970) was used to prepare microscope slides. Images were acquired using 100x objective on a Leica TCS SP8 confocal microscope. All specimens with same staining antibodies were imaged under identical conditions and analyzed with identical parameters using Image J software (version 1.52p, NIH). PL in medial PFC was selected as the area of interest for comparisons.

2.6. Chromatin immunoprecipitation (CHIP)

As described previously (Qin et al., 2021; Wang et al., 2020), bilateral PFC was collected. Each sample was homogenized in 250 μl ice cold douncing buffer (10 mM Tris-HCl, pH 7.5, 4 mM $MgCl_2$, 1 mM $CaCl_2$) with 1 ml 26-gauge syringe for 15 times. The homogenized sample was incubated with micrococcal nuclease (5 U/ml, Sigma, N5386) for 7 min at 37 °C and terminated by adding EDTA (10 mM, Invitrogen, 15575-038). Then, 1 ml hypotonic lysis buffer (0.2 mM EDTA, pH 8.0, 0.1 mM benzamidine, 0.1 mM PMSF, 1.5 mM DTT) containing protease inhibitor was added and incubated on ice for 1 h with brief vortex at 10

min intervals. The supernatant was transferred to a new tube after centrifugation (3000 g for 5 min at 4 °C). After adding 10 × incubation buffer (50 mM EDTA, 200 mM Tris-HCl, 500 mM NaCl), 5–10% of the supernatant was saved to serve as input control.

To reduce nonspecific background, the supernatant was pre-cleared with 100 μl of salmon sperm DNA/protein A agarose-50% slurry (Millipore, 16–157) for 2 h at 4 °C with agitation. The pre-cleared supernatant was incubated with antibodies against H3K9me2 (8 μg per reaction; cell signaling, 4658) or Rabbit IgG (8 μg per reaction; sigma-Aldrich, 12–370) overnight at 4 °C under constant rotation, followed by incubation with 60 μl of Salmon Sperm DNA/Protein A agarose 50% Slurry for 2 h at 4 °C. After washing with Low salt wash buffer, High salt wash buffer, LiCl wash buffer and TE buffer (twice), bound complex was eluted twice from the beads by incubating with the elution buffer (1% SDS, 0.1 M $NaHCO_3$, 100 μl) at room temperature. 5M NaCl (8 μl), 0.5M EDTA (4 μl), 1M Tris-HCl (pH 7.4, 8 μl), and 20 mg/ml proteinase K (0.4 μl, Thermo Fisher, EO0491) were used to combine eluates and incubate for 1 h at 50 °C. Then immunoprecipitated DNA and input DNA were purified by QIAquick PCR purification Kit (Qiagen, 28104). The 30 μl Buffer EB (Qiagen, 19086) was used for DNA dissolution. Quantification of ChIP signals was calculated as % input.

Purified DNA was subjected to qPCR reactions with primers against mouse Arc enhancer (Primer1, Forward, 9066–9085 bp relative to transcription start site (TSS), 5′-GGTGCATAACACTGGCAAGC-3’; Reverse, 9171–9190 bp relative to TSS, 5′- ATCTCTAGGTCGGGGTCCTG -3’. Primer2, Forward, 10323-10342 bp relative to TSS, 5′- ACTC-CACTCTGAGCCTGACAA -3’; Reverse, 10491-10510 bp relative to TSS, 5′- ACAGGTGTTTTGGGAGTGGTA-3’. Primer3, Forward, 11447-11466 bp relative to TSS, 5′- CCACTCCAGCTGTGGTGTTA -3’; Reverse, 11542-11561 bp relative to TSS, 5′-CCTCTAGGCTTCCCCAGGAT -3′). PCR cycling parameters are 95 °C for 3 min followed by 40 cycles of 95 °C for 15 s, 58 °C for 30 s.

2.7. Statistics

Statistical analysis was performed using GraphPad Prism 8.4.3. Data were tested for normality before parametric analysis. Shapiro-Wilk test was used to test for normality. The comparisons between two independent groups were analyzed using two-tailed unpaired t-tests when the data were normally distributed, otherwise Mann-Whitney (M-W) test was used. The comparisons among more than two groups were analyzed using ANOVA when the data had normal distribution and homogeneity

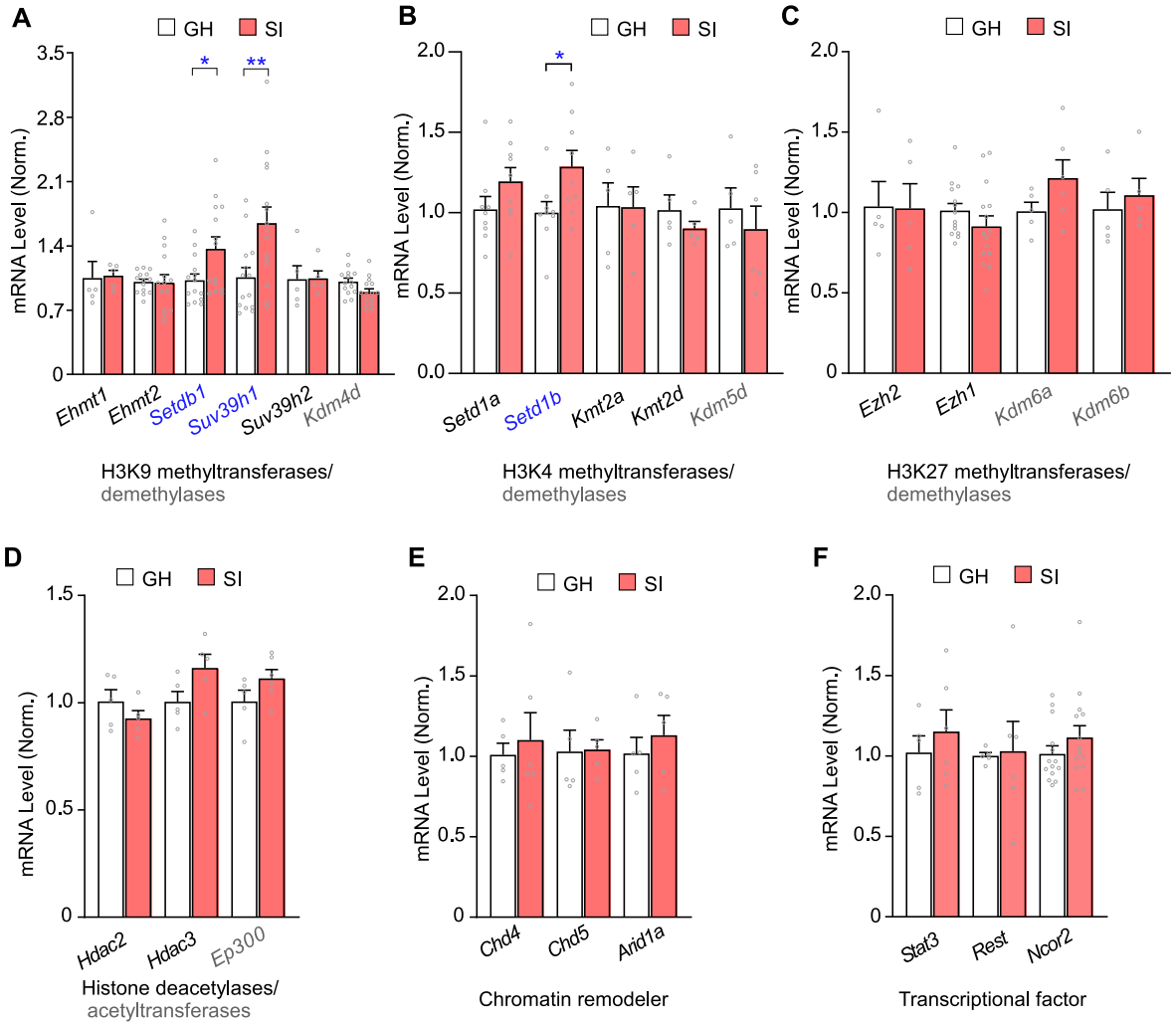

Fig. 1. H3K9 methyltransferases were selectively increased in PFC of female mice exposed to chronic adolescent social isolation stress. A-C. Quantitative PCR data showing the mRNA level of histone methyltransferases and demethylases *for* H3K9 (A, *Ehmt1/2*, *Setdb1*, *Suv39h1/2, Kdm4d*), H3K4 (B, *Setd1a/b*, *Kmt2a*/d, *Kdm5d*), and H3K27 (C, *Ezh1/2*, *Kdm6a/b*) in PFC of group-housed (GH) vs. socially isolated (SI) female mice (GH, n = 5–14; SI, n = 5–15). A, B, $^*P < 0.05$, $^{**}P < 0.01$, unpaired *t*-test. **D.** Quantitative PCR data showing the mRNA level of histone acetyltransferases and deacetylases *(Ep300*, *Hdac2,3)* in PFC of GH and SI mice (GH, n = 5; SI, n = 5–6). **E, F.** Quantitative PCR data showing the mRNA level of chromatin remodelers (E, *Chd4,5*, *Arid1a*) and transcriptional factors (F, *Stat3*, *Rest*, *Ncor2)* in PFC of GH and SI mice (E: GH, n = 5; SI, n = 5–6; F: GH, n = 5–14; SI, n = 5–14). All data are expressed as mean ± SEM.

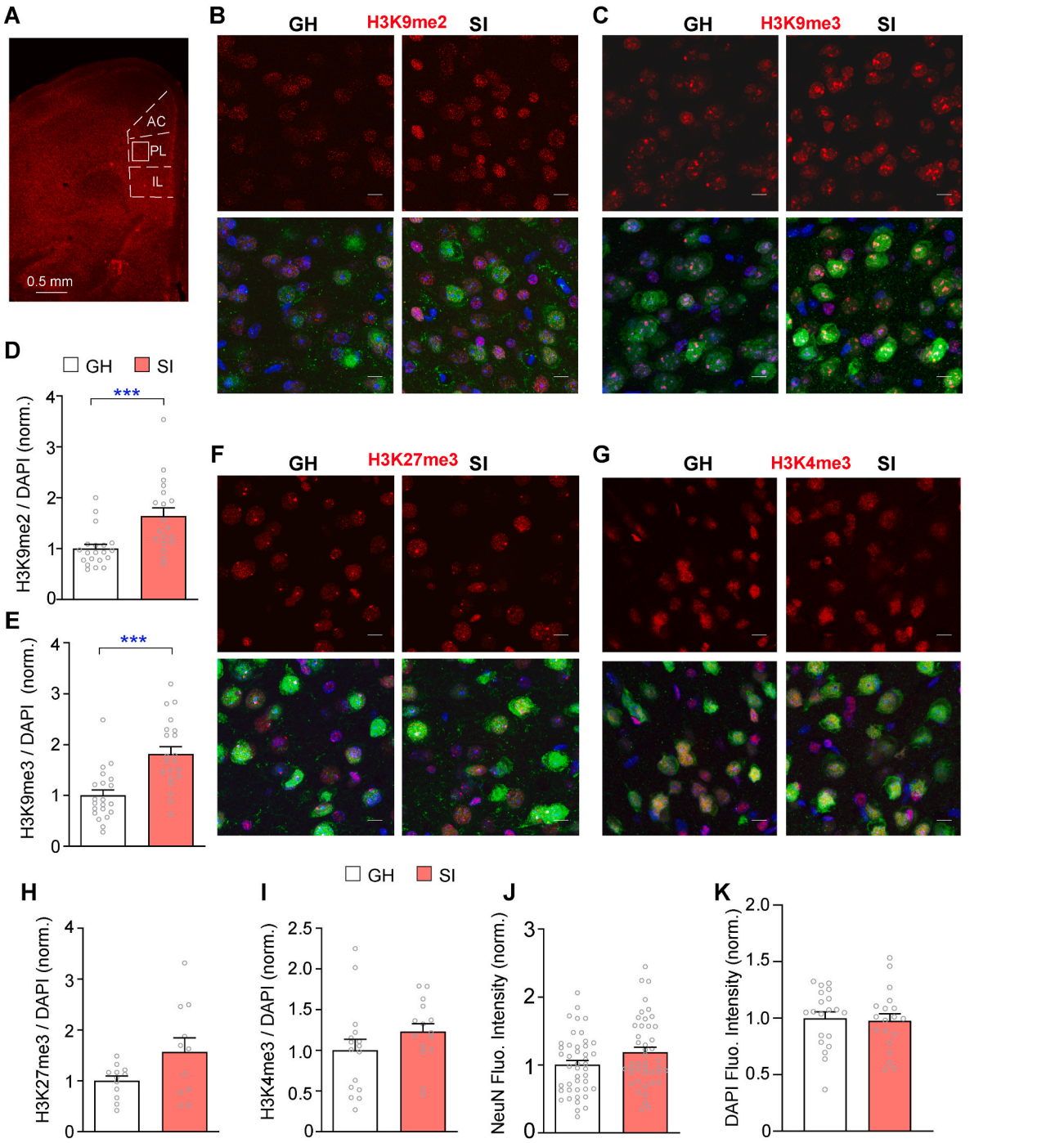

Fig. 2. H3K9 methylation were increased in PFC of female mice exposed to chronic adolescent social isolation stress. A, A low-magnification (2x) image showing the location of immunostained cells. The boxed area in PL is the region for imaging and analyses. **B, C,** Representative confocal images (100x) of immunostaining of H3K9me2 (red) and H3K9me3 (red) in PFC of GH and SI mice. Bottom rows are merged images of H3K9me2/3 (red) with NeuN (Green) and DAPI (blue). Scale bars: 10 μm. **D, E,** Quantification of H3K9me2 and H3K9me3 fluorescent intensity (normalized with DAPI) in PFC of GH and SI mice (n = 19–20 images/4 mice/group). ***$P < 0.001$, unpaired *t*-test (H3K9me3) or M-W test (H3K9me2). **F, G,** Representative confocal images of immunostaining of H3K27me3 (red) and H3K4me3 (red) in PFC of GH and SI mice. Bottom rows are merged images of H3K27me3 or H3K4me3 (red) with NeuN (Green) and DAPI (blue). Scale bars: 10 μm. **H, I,** Quantification of H3K27me3 and H3K4me3 fluorescent intensity (normalized with DAPI) in PFC of GH and SI mice (n = 11–16 images/4 mice/group). **J, K,** Quantification of NeuN and DAPI fluorescent intensity in PFC of GH and SI mice (NeuN, n = 44–45 images/4 mice/group; DAPI, n = 19–20 images/4 mice/group). All data are expressed as mean ± SEM.

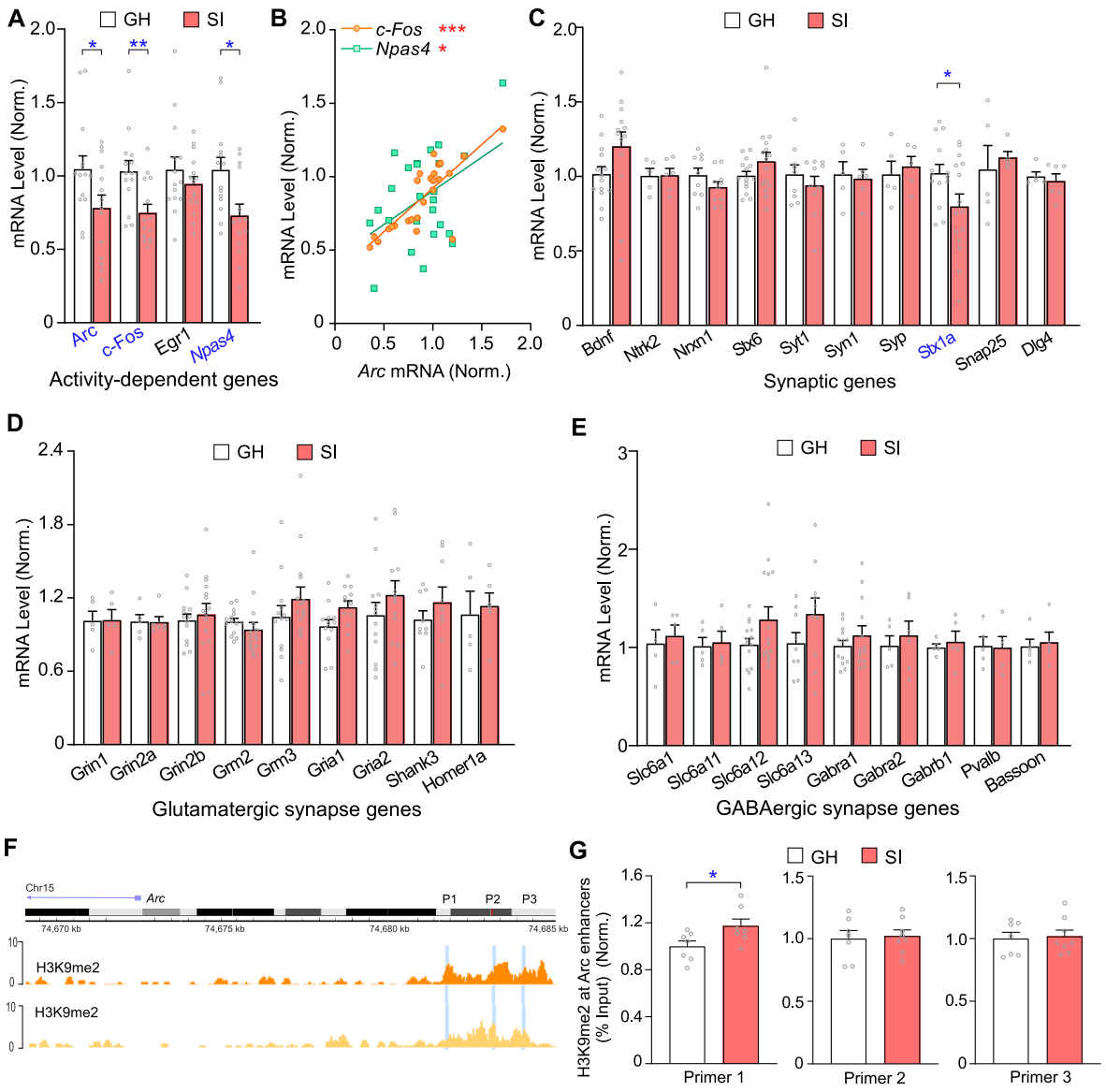

Fig. 3. Activity-dependent synaptic plasticity gene *Arc* was reduced in PFC of SI females, which was correlated with the increased H3K9me2 occupancy at its enhancer. A. Quantitative PCR data showing the mRNA level of activity-dependent immediate early genes (*Arc*, *c-Fos*, *Egr1*) or transcription factor (*Npas4*) in PFC of GH and SI mice (GH, n = 14; SI, n = 14–16). **B.** Pearson's correlation analysis between the mRNA level of *Arc* and *c-Fos* or *Npas4* (n = 25) in female mice. **C-E.** Quantitative PCR data showing the mRNA level of synaptic genes involved in presynaptic transmitter release (C), glutamatergic synapses (D) or GABAergic synapses (E) in PFC of GH and SI mice (GH, n = 5–15; SI, n = 5–16). **F.** Diagram showing the occupancy of H3K9me2 at *Arc* enhancer region and the location of primers used in CHIP assays (light blue rectangular area). **G.** CHIP assay data showing the enrichment of H3K9me2 at *Arc* enhancer regions in PFC of GH and SI mice (GH, n = 7, SI, n = 6). A, C, G, $^{*}P < 0.05$, $^{**}P < 0.01$, unpaired *t*-test. All data are expressed as mean ± SEM.

of variance, otherwise Kruskal-Wallis test was used with Dunn's multiple *post hoc* comparisons. Pearson's correlation analysis was conducted for correlation analysis. All data were presented as the mean ± SEM.

3. Results

3.1. Repressive H3K9 methylation is elevated in PFC of female mice exposed to adolescent social isolation stress

Our previous studies reported that adolescent social isolation (SI) stress had sex-specific effects (Tan et al., 2021; Wang et al., 2022b). Because females are found to be more susceptible to anxiety disorders (Dalla et al., 2005; Wellman et al., 2018), we focused on SI females in this study. Stress-related disorders are linked to disrupted epigenetic regulation of gene expression (Sanacora et al., 2022), so we screened the expression of epigenetic enzymes that control histone methylation and acetylation with qPCR.

We first examined the principal members of histone methyltransferases (HMTs) catalyzing repressive H3K9 methylation, *Ehmt1/2, Setdb1* and *Suv39h1/2* (Padeken et al., 2022). A significant increase of *Setdb1* and *Suv39h1* mRNAs was found in PFC of SI females, compared to group-housed (GH) controls (Fig. 1A, GH: n = 14, SI: n = 14–15, *Setdb1*, $t_{(26)} = -2.34$, $P = 0.027$; *Suv39h1*, $t_{(27)} = -2.85$, $P = 0.008$; unpaired *t*-test). Other H3K9 HMTs, including *Ehmt1/2* and *Suv39h2*, as well as H3K9 demethylase *Kdm4d*, were not significantly changed.

We next tested the mRNA level of HMTs catalyzing permissive H3K4 methylation, *Setd1a/b* and *Kmt2a/d*, as well as the H3K4 HDM *Kdm5d*. No significant changes were found on these genes between GH and SI groups, except for *Setd1b* (n = 9 pairs, $t_{(14)} = 2.32$, $P = 0.036$; unpaired *t*-test) (Fig. 1B). The mRNA level of *Ezh1/2* and *Kdm6a/b* (HMTs and HDMs for repressive H3K27 methylation, respectively) was also unchanged (Fig. 1C).

In addition, we examined the expression of histone acetyltransferase *Ep300* and histone deacetylases *Hdac2/3* (Fig. 1D), chromatin remodelers *Chd4/5* and *Arid1a* (Fig. 1E), and transcriptional factors *Stat3*, *Rest*, and *Ncor2* (Fig. 1F). No significant change was found on these genes.

To verify the change of H3K9 methylation after chronic social isolation, we performed immunostaining of methylated H3K9 in PFC slices (Fig. 2A). As shown in Fig. 2B-E, the fluorescent signal of H3K9 dimethylation (H3K9me2) and tri-methylation (H3K9me3) were significantly elevated in PFC neurons of SI females, compared to GH controls (H3K9me2, GH: n = 20, SI: n = 19, $P = 0.0003$; M-W test; H3K9me3, GH: n = 21, SI: n = 21, $t_{(40)} = -4.42$, $P < 0.0001$; unpaired *t*-test), while the fluorescent signal of H3K27me3 and H3K4me3 was not significantly changed (Fig. 2F-I). The number of NeuN positive or DAPI positive cells was unchanged (Fig. 2J and **K**), indicating the lack of neuron loss after chronic social isolation. Taken together, these data suggest that adolescent social isolation stress selectively elevates repressive H3K9 methylation in PFC of female mice.

3.2. Expression of activity-dependent genes is reduced in PFC of female mice exposed to adolescent social isolation stress

Next, we examined potential downstream genes that may be affected

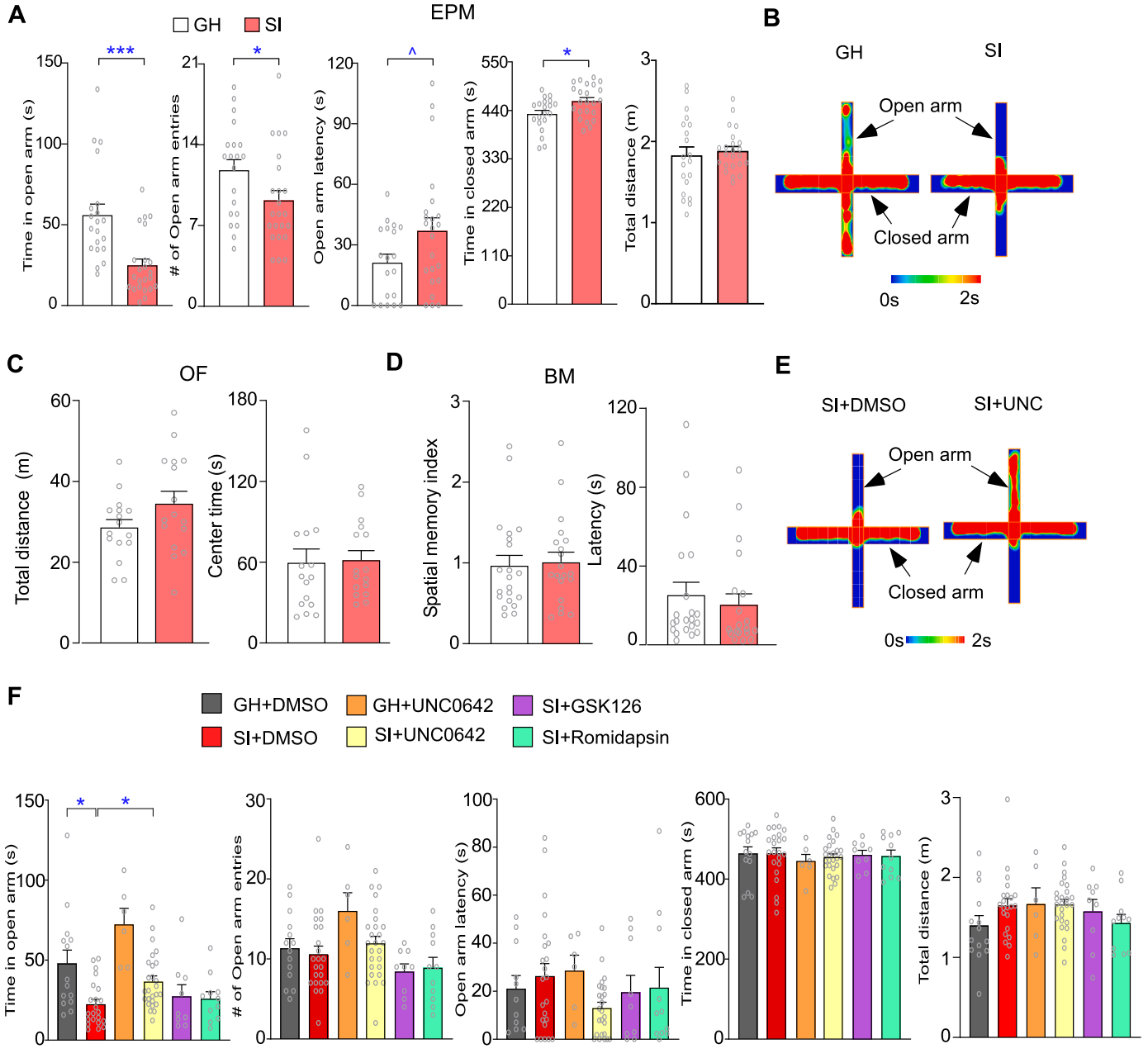

Fig. 4. H3K9 methylation inhibitor UNC0642 alleviated anxiety-like behavior in SI females. A. Bar graphs showing parameters of elevated plus maze (EPM) tests (time in open and closed arms, number of entries to open arms, latency to open arms, and total distance traveled) in GH and SI females (GH, n = 20; SI, n = 23). ^ $P < 0.1$, *$P < 0.05$, ***$P < 0.001$, M-W test (open arm time, entry and latency), unpaired *t*-test (closed arm time). **B.** Representative heatmaps showing the time spent in EPM arena of a GH and a SI mouse. **C.** Bar graphs showing the total distance and the time in center area open field (OF) tests (GH, n = 16; SI, n = 16). **D.** Bar graphs showing the spatial memory index and latency to correct hole in Barnes Maze (BM) tests (GH, n = 21; SI, n = 20). **E.** Representative heatmaps of EPM tests of SI females treated with DMSO or UNC0642. **F.** Bar graphs of EPM parameters in GH or SI females treated with DMSO, UNC0642 (Ehmt1/2 inhibitor), GSK126 (Ezh2 inhibitor), or Romidepsin (class I Hdac inhibitor) (GH + DMSO, n = 14; SI + DMSO, n = 22; GH + UNC, n = 6; SI + UNC, n = 26; SI + GSK, n = 9, SI + Romidepsin, n = 11). *$P < 0.05$, Kruskal-Wallis test with Dunn's multiple comparisons. All data were expressed as mean ± SEM.

by the elevated of H3K9 methylation in PFC of SI females. Considering the disruption of PFC neuronal activity by chronic social isolation (Tan et al., 2021), the first set of candidates we tested was activity-dependent immediate early genes (IEGs) or transcription factors, *Arc, c-Fos, Egr1* and *Npas4*, which play an important role in synaptic processes critical for key brain functions (Kim et al., 2018). As shown in Fig. 3A, *Arc, c-Fos* and *Npas4* mRNA levels were significantly lower in SI mice, compared to GH mice (GH: n = 14, SI: n = 14, *Arc*, $t_{(26)} = 2.1$, $P = 0.046$; c-*Fos*, $t_{(26)} = 3.04$, $P = 0.005$; *Npas4,* $t_{(26)} = 2.71$, $P = 0.012$; unpaired *t*-test), while *Egr1* was unchanged. Pearson's correlation analysis found significant positive correlations between *Arc* and *c-Fos* or *Npas4* (Fig. 3B, *c-Fos*, n = 25, $P < 0.001$; *Npas4*, n = 25, $P = 0.024$).

Given the significance of synaptic dysfunction in neuropsychiatric disorders (van Spronsen and Hoogenraad, 2010), we next examined genes directly related to synaptic function. As shown in Fig. 3C, *Bdnf* (encoding Brain derived neurotrophic factor BDNF) and its receptor *Ntrk2* (encoding Neurotrophic receptor tyrosine kinase 2, NTRK2), *Stx6* (encoding Syntaxin 6), *Syt1* (encoding Synaptotagmin 1), *Syn1* (encoding Synapsin I), *Syp* (encoding Synaptophysin), *Snap25* (encoding Synaptosome associated protein 25, SNAP25), and *Dlg4* (encoding PSD-95) all showed no significant changes. Only *Stx1a*, a vital component of the SNARE complex that plays a crucial role in neurotransmitter release (Vardar et al., 2016), exhibited a significant decrease in PFC of SI females (GH: n = 14, SI: n = 15, $t_{(27)} = 2.17$, $P = 0.039$; unpaired *t*-test).

Prior studies have found that EHMT1/2-mediated H3K9 methylation can regulate genes related to synaptic dysfunction (Benevento et al., 2016; Gupta-Agarwal et al., 2012; Maze et al., 2010; Wang et al., 2020; Zheng et al., 2019), so we also investigated the expression of genes related to glutamatergic synapses in PFC of SI females. As depicted in Fig. 3D, there were no significant alterations in the mRNA level of NMDAR subunits *Grin1* and *Grin2a/2b* (encoding NR1 and NR2A/2B), Group II metabotropic glutamate receptors Grm2/3 (encoding mGluR2/3), AMPAR subunits *Gria1/2* (encoding GluR1/2), *Shank3* (encoding scaffolding protein Shank3), and *Homer1a* (encoding mGluR anchoring protein Homer1a). Similarly, no significant changes were observed for GABAergic inhibitory synaptic genes, including GABA transporters *Slc6a1/11/12/13* (encoding GAT1, GAT2, BGT1 and GAT3), $GABA_AR$ subunits *Gabra1/a2/b1* (encoding $GABA_AR$ α1/α2/β1), *Pvalb* (encoding Parvalbumin), and *Bassoon* (encoding presynaptic scaffold protein Bassoon) (Fig. 3E). These results suggest that adolescent social isolation does not affect the transcription of most glutamatergic and GABAergic synaptic genes in PFC of SI female mice.

To address the molecular link between altered H3K9 methylation and gene expression in PFC of SI females, we performed CHIP assay to examine H3K9me2 occupancy at the enhancer region of *Arc* gene. As illustrated in the Genome browser snapshots of H3K9me2 (GSE 153651), H3K9me2 has the most prominent occupancy at *Arc* enhancer (9 Kb relative to TSS) (Fig. 3F). SI females had significantly increased H3K9me2 occupancy at an enhancer region of *Arc* (Fig. 3G, GH: n = 7, SI: n = 6, $t_{(11)} = -2.37$, $P = 0.037$; unpaired *t*-test). It suggests that the reduced Arc expression could be caused by the increased binding of repressive H3K9me2 to its enhancer in PFC of SI mice.

3.3. Inhibition of H3K9 methylation alleviates anxiety-related behavior and restores activity-dependent gene expression in stressed females

Next, we tried to find out the therapeutic potential of targeting the epigenetic abnormality in SI females. To test this, we first performed a set of behavioral assays to measure emotional and cognitive processes. Elevated plus maze (EPM) tests were used to detect anxiety-related behaviors. As shown in Fig. 4A and B, SI females exhibited the significantly reduced exploration time in open arms (GH: n = 20, SI: n = 23, $P < 0.001$; M-W test), the decreased entries into open arms ($P < 0.05$; M-W test), a prolonged latency to enter the open arms ($P = 0.06$; M-W test), the increased exploration time in closed arms ($t_{(41)} = -2.58$, $P = 0.014$; unpaired *t*-test), and no change in total distance, suggesting the elevated level of anxiety. In open-field (OF) tests, SI females did not show significant changes in total distance or time in center, compared to GH mice (Fig. 4C). Barnes maze (BM), a behavioral task for spatial memory, was also compared. As shown Fig. 4D, spatial memory index and the latency to the correct hole showed no difference between GH vs. SI females. These results suggest that chronic adolescent social isolation induces anxiety in female mice.

To determine whether reducing H3K9 methylation can rescue anxiety caused by chronic social isolation, we intraperitoneally (i.p.) administered a highly selective EHMT inhibitor (Liu et al., 2013), UNC0642 (1 mg/kg bw, once a day for three consecutive days) (Wang et al., 2021), in SI females. Behavior tests were conducted 24 h after the last UNC0642 administration. As shown in Fig. 4E and **F**, compared to DMSO-injected SI mice, treatment of SI mice with UNC0642 alleviated anxiety, which was reflected by the significantly increased exploration time in open arms (SI + DMSO: n = 22, SI + UNC: n = 26, $P = 0.028$, K–W test), the increased trend of open arm entries and the reduced trend of latency to open arms.

To test the specificity of the therapeutic effect of UNC0642, we also examined Ezh2 (HMT of H3K27) inhibitor GSK126 (0.5 mg/kg.bw, i.p., 3x) and class I selective Hdac inhibitor Romidepsin (0.25 mg/kg.bw, i.p., 3x). As shown in Fig. 4E, neither GSK126 nor Romidepsin could alleviate SI-induced anxiety. These data suggest that the increased H3K9 methylation is specifically linked to anxiety after chronic social isolation.

We next examined the potential mechanism underlying the

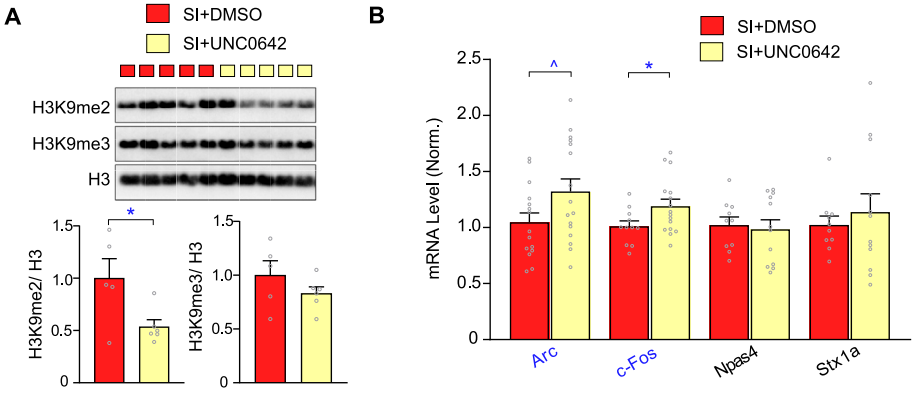

Fig. 5. UNC0642 treatment reduced H3K9me2 and increased *Arc* expression in PFC of SI females. A. Representative and quantitation of immunoblots of H3K9me2 and H3K9me3 protein levels in the nuclear fraction of PFC from SI mice treated with DMSO or UNC0642 (SI + DMSO, n = 5, SI + UNC, n = 6). *$P < 0.05$, unpaired *t*-test. **B.** Quantitative PCR data showing the mRNA level of *Arc*, *c-Fos*, *Npas4* and *Stx1a* in SI mice treated with DMSO or UNC0642 (SI + DMSO, n = 10–16, SI + UNC, n = 12–16). ^ $P < 0.1$, *$P < 0.05$, unpaired *t*-test. All data are expressed as mean ± SEM.

behavioral rescue of UNC0642. Western blot analyses (Fig. 5A) indicated the significantly decreased H3K9me2 in PFC of UNC0642-treated SI mice (SI + DMSO: n = 5, SI + UNC: n = 6, $t_{(9)} = 2.52$, $P = 0.033$, unpaired *t*-test), confirming the effectiveness of UNC0642 on H3K9 methylation in the brain. Quantitative PCR showed that UNC treatment elevated the expression of *Arc* and *c-Fos* (Fig. 5B, *Arc*, SI + DMSO: n = 15, SI + UNC: n = 16, $t_{(29)} = -1.93$, $P = 0.063$; *C-Fos*, SI + DMSO: n = 11, SI + UNC: n = 16, $t_{(25)} = -2.09$, $P = 0.047$, unpaired *t*-test). The restoration of these activity-dependent IEGs by UNC0642 may contribute to the alleviation of anxiety in SI mice.

4. Discussion

Stress is an important environmental factor that can trigger epigenetic changes, including histone modifications that play a key role in regulating gene activation or silencing (Stillman, 2018). Increased histone acetylation was found in nucleus accumbens after prolonged social defeat stress (Covington et al., 2009). Restraint stress was found to alter the methylation of H3K9, H3K27, and H3K4 in dentate gyrus (DG) and CA1 regions of hippocampus in a time-dependent manner: acute or 1-week restraint stress increased H3K9me3 levels, while 3-week restraint stress reduced H3K9me3 in DG (Hunter et al., 2009). Eight-week social isolation in adult male mice led to decreased H3K9me3 expression in PFC oligodendrocytes, causing impaired myelination (Liu et al., 2016). In the current study, we found that repressive H3K9 methylation and H3K9 methyltransferases, SUV39H1 and SETDB1, were specifically increased in PFC of female mice exposed to 6-week adolescent social isolation stress. These data underscore the importance of H3K9 methylation in stress responses, suggesting that targeting H3K9-catalyzing enzymes could be a therapeutic avenue to mitigate behavioral abnormalities following stress.

H3K9 methylation has been found to regulate the transcription of genes involved in synaptic networks (Benevento et al., 2016; Gupta-Agarwal et al., 2012; Maze et al., 2010). In searching of potential downstream genes affected by the elevated H3K9 methylation in PFC of SI females, we found the significantly decreased expression of activity-dependent immediate early genes (IEGs), including *Arc*, *c-Fos,* and *Npas4*, consistent with a prior finding (Ieraci et al., 2016). IEGs play a crucial role in regulating synaptic plasticity, synapse formation, and memory-encoding neuronal ensembles (Minatohara et al., 2015; Sun and Lin, 2016). Disruption of Arc in mice led to the manifestation of schizophrenia-related behavioral phenotypes and hypoactive mesocortical pathways (Managò et al., 2016). The transcriptional level of *Arc* gene is regulated by synaptic activity (Guzowski et al., 1999): suppression of neuronal activity decreases Arc protein, while elevation of neuronal activity enhances *Arc* expression (Korb et al., 2013; Saha et al., 2011; Shepherd et al., 2006). Thus, the decrease of activity-dependent genes in SI females could be due to the reduced PFC activity (Tan et al., 2021; Wang et al., 2022b). While no transcriptional changes in glutamatergic or GABAergic genes are found in SI females, the altered expression of Arc could lead to changes in PFC synaptic function via regulating AMPAR endocytosis (Chowdhury et al., 2006; Rial Verde et al., 2006) or NMDAR activity (Chowdhury et al., 2006; Wang et al., 2020). Our ChIP assays have revealed the increased H3K9me2 occupancy at *Arc* enhancer in SI females, correlated with the reduced *Arc* expression, further suggesting that *Arc* transcription can be regulated by H3K9 methylation (Wang et al., 2020).

With the identification of increased H3K9 methylation in PFC of SI females, we tested the therapeutic potential of UNC0642, a specific inhibitor of H3K9 methyltransferases Ehmt1/2. Our behavioral assays found that SI females exhibited elevated anxiety, which was relieved by a short treatment with UNC0642. In contrast, other epigenetic drugs targeting different histone modifying enzymes, such as Ezh2 and Hdac, were not effective. One thing worth noting is that in the SI group, we reduced an enrichment component and covered the cage to prevent visual contact with other animals. The reason of doing these is to provide an environment more closely mimicking social isolation that is often associated with impoverished setting and deprivation of visual cues. While environmental enrichment and sensory stimulation can influence animal behaviors, including cognitive function, emotional well-being, and neural plasticity (Laviola et al., 2008; Nithianantharajah and Hannan, 2006; Simpson and Kelly, 2011; van Praag et al., 2000), our previous studies without changing enrichment or blocking visual cues found similarly elevated anxiety in SI females (Tan et al., 2021; Wang et al., 2020). Thus, it is unlikely that the behavioral differences observed here between GH and SI animals are mainly caused by the change of enrichment or visual cues.

Human functional imaging studies have found that the higher strength of amygdala-prefrontal pathway is related to lower anxiety level (Kim and Whalen, 2009), and ACC in PFC constitutes a hub to process and regulate negative affect and anxiety (Shackman et al., 2011). UNC0642 elevated the expression of *Arc* and *c-Fos* in PFC of SI females. Given the role of Arc as a multifunctional and interactive master organizer for synaptic plasticity (Nikolaienko et al., 2018), restoration of Arc expression by UNC0642 treatment may lead to the normalization of synaptic activity of PFC and its control of amygdala, which contributes to the rescuing effects of UNC0642 on anxiety-related behaviors.

Chronic social isolation during adolescence is strongly linked to mental impairment (Sun et al., 2017; Tan et al., 2021; Wang et al., 2022b; Zelikowsky et al., 2018). Anxiety disorders rank among the most prevalent conditions affecting adolescents. The current study has revealed an epigenetic mechanism and treatment strategy for isolation stress-induced anxiety and related abnormalities.

CRediT authorship contribution statement

Pei Li: Data curation, Formal analysis, Writing – original draft. **Zhen Yan:** Conceptualization, Supervision, Writing – review & editing.

Declaration of competing interest

The authors declare no competing interests.

Data availability

Data will be made available on request.

Acknowledgements

We thank Xiaoqing Chen for her excellent technical support, Dr. Yong Ren for his help in CHIP assay, Dr. Qing Cao for her help in Western blotting and immunostaining, Dr. Kelcie Schatz and Dr. Megan Conrow for their help in behavior tests. This work was supported by grants from the National Institutes of Health (MH126443 and NS127728) to Z.Y.

References

Benevento, M., Iacono, G., Selten, M., Ba, W., Oudakker, A., Frega, M., Keller, J., Mancini, R., Lewerissa, E., Kleefstra, T., et al., 2016. Histone methylation by the kleefstra syndrome protein EHMT1 mediates homeostatic synaptic scaling. Neuron 91, 341–355.

Cao, Q., Wang, W., Williams, J.B., Yang, F., Wang, Z.J., Yan, Z., 2020. Targeting histone K4 trimethylation for treatment of cognitive and synaptic deficits in mouse models of Alzheimer's disease. Sci. Adv. 6.

Carlén, M., 2017. What constitutes the prefrontal cortex? Science 358, 478–482.

Chowdhury, S., Shepherd, J.D., Okuno, H., Lyford, G., Petralia, R.S., Plath, N., Kuhl, D., Huganir, R.L., Worley, P.F., 2006. Arc/Arg3.1 interacts with the endocytic machinery to regulate AMPA receptor trafficking. Neuron 52, 445–459.

Covington, H.E., Maze, I., LaPlant, Q.C., Vialou, V.F., Ohnishi, Y.N., Berton, O., Fass, D. M., Renthal, W., Rush, A.J., Wu, E.Y., et al., 2009. Antidepressant actions of histone deacetylase inhibitors. J. Neurosci. 29, 11451–11460.

Dalla, C., Antoniou, K., Drossopoulou, G., Xagoraris, M., Kokras, N., Sfikakis, A., Papadopoulou-Daifoti, Z., 2005. Chronic mild stress impact: are females more vulnerable? Neuroscience 135, 703–714.

Franklin, T.B., Silva, B.A., Perova, Z., Marrone, L., Masferrer, M.E., Zhan, Y., Kaplan, A., Greetham, L., Verrechia, V., Halman, A., et al., 2017. Prefrontal cortical control of a brainstem social behavior circuit. Nat. Neurosci. 20, 260–270.
Gupta-Agarwal, S., Franklin, A.V., Deramus, T., Wheelock, M., Davis, R.L., McMahon, L. L., Lubin, F.D., 2012. G9a/GLP histone lysine dimethyltransferase complex activity in the hippocampus and the entorhinal cortex is required for gene activation and silencing during memory consolidation. J. Neurosci. 32, 5440–5453.
Guzowski, J.F., McNaughton, B.L., Barnes, C.A., Worley, P.F., 1999. Environment-specific expression of the immediate-early gene Arc in hippocampal neuronal ensembles. Nat. Neurosci. 2, 1120–1124.
Hare, B.D., Duman, R.S., 2020. Prefrontal cortex circuits in depression and anxiety: contribution of discrete neuronal populations and target regions. Mol. Psychiatr. 25, 2742–2758.
Hunter, R.G., McCarthy, K.J., Milne, T.A., Pfaff, D.W., McEwen, B.S., 2009. Regulation of hippocampal H3 histone methylation by acute and chronic stress. Proc. Natl. Acad. Sci. U.S.A. 106, 20912–20917.
Ieraci, A., Mallei, A., Popoli, M., 2016. Social isolation stress induces anxious-depressive-like behavior and alterations of neuroplasticity-related genes in adult male mice. Neural Plast., 6212983, 2016.
Kim, M.J., Whalen, P.J., 2009. The structural integrity of an amygdala-prefrontal pathway predicts trait anxiety. J. Neurosci. 29, 11614–11618.
Kim, S., Kim, H., Um, J.W., 2018. Synapse development organized by neuronal activity-regulated immediate-early genes. Exp. Mol. Med. 50, 1–7.
Korb, E., Wilkinson, C.L., Delgado, R.N., Lovero, K.L., Finkbeiner, S., 2013. Arc in the nucleus regulates PML-dependent GluA1 transcription and homeostatic plasticity. Nat. Neurosci. 16, 874–883.
Kundakovic, M., Lim, S., Gudsnuk, K., Champagne, F.A., 2013. Sex-specific and strain-dependent effects of early life adversity on behavioral and epigenetic outcomes. Front. Psychiatr. 4, 78.
Laviola, G., Hannan, A.J., Macrì, S., Solinas, M., Jaber, M., 2008. Effects of enriched environment on animal models of neurodegenerative diseases and psychiatric disorders. Neurobiol. Dis. 31, 159–168.
Lee, C.R., Chen, A., Tye, K.M., 2021. The neural circuitry of social homeostasis: consequences of acute versus chronic social isolation. Cell 184, 1500–1516.
Liu, F., Barsyte-Lovejoy, D., Li, F., Xiong, Y., Korboukh, V., Huang, X.P., Allali-Hassani, A., Janzen, W.P., Roth, B.L., Frye, S.V., et al., 2013. Discovery of an in vivo chemical probe of the lysine methyltransferases G9a and GLP. J. Med. Chem. 56, 8931–8942.
Liu, J., Dupree, J.L., Gacias, M., Frawley, R., Sikder, T., Naik, P., Casaccia, P., 2016. Clemastine enhances myelination in the prefrontal cortex and rescues behavioral changes in socially isolated mice. J. Neurosci. 36, 957–962.
Loades, M.E., Chatburn, E., Higson-Sweeney, N., Reynolds, S., Shafran, R., Brigden, A., Linney, C., McManus, M.N., Borwick, C., Crawley, E., 2020. Rapid systematic review: the impact of social isolation and loneliness on the mental health of children and adolescents in the context of COVID-19. J. Am. Acad. Child Adolesc. Psychiatry 59, 1218–1239 e1213.
Managò, F., Mereu, M., Mastwal, S., Mastrogiacomo, R., Scheggia, D., Emanuele, M., De Luca, M.A., Weinberger, D.R., Wang, K.H., Papaleo, F., 2016. Genetic disruption of Arc/Arg3.1 in mice causes alterations in dopamine and neurobehavioral phenotypes related to schizophrenia. Cell Rep. 16, 2116–2128.
Maze, I., Covington 3rd, H.E., Dietz, D.M., LaPlant, Q., Renthal, W., Russo, S.J., Mechanic, M., Mouzon, E., Neve, R.L., Haggarty, S.J., et al., 2010. Essential role of the histone methyltransferase G9a in cocaine-induced plasticity. Science 327, 213–216.
Minatohara, K., Akiyoshi, M., Okuno, H., 2015. Role of immediate-early genes in synaptic plasticity and neuronal ensembles underlying the memory trace. Front. Mol. Neurosci. 8, 78.
Nikolaienko, O., Patil, S., Eriksen, M.S., Bramham, C.R., 2018. Arc protein: a flexible hub for synaptic plasticity and cognition. Semin. Cell Dev. Biol. 77, 33–42.
Nithianantharajah, J., Hannan, A.J., 2006. Enriched environments, experience-dependent plasticity and disorders of the nervous system. Nat. Rev. Neurosci. 7, 697–709.
Padeken, J., Methot, S.P., Gasser, S.M., 2022. Establishment of H3K9-methylated heterochromatin and its functions in tissue differentiation and maintenance. Nat. Rev. Mol. Cell Biol. 23, 623–640.
Qin, L., Williams, J.B., Tan, T., Liu, T., Cao, Q., Ma, K., Yan, Z., 2021. Deficiency of autism risk factor ASH1L in prefrontal cortex induces epigenetic aberrations and seizures. Nat. Commun. 12, 6589.
Reinert, S., Hübener, M., Bonhoeffer, T., Goltstein, P.M., 2021. Mouse prefrontal cortex represents learned rules for categorization. Nature 593, 411–417.
Rial Verde, E.M., Lee-Osbourne, J., Worley, P.F., Malinow, R., Cline, H.T., 2006. Increased expression of the immediate-early gene arc/arg3.1 reduces AMPA receptor-mediated synaptic transmission. Neuron 52, 461–474.
Saha, R.N., Wissink, E.M., Bailey, E.R., Zhao, M., Fargo, D.C., Hwang, J.Y., Daigle, K.R., Fenn, J.D., Adelman, K., Dudek, S.M., 2011. Rapid activity-induced transcription of Arc and other IEGs relies on poised RNA polymerase II. Nat. Neurosci. 14, 848–856.
Sanacora, G., Yan, Z., Popoli, M., 2022. The stressed synapse 2.0: pathophysiological mechanisms in stress-related neuropsychiatric disorders. Nat. Rev. Neurosci. 23, 86–103.
Shackman, A.J., Salomons, T.V., Slagter, H.A., Fox, A.S., Winter, J.J., Davidson, R.J., 2011. The integration of negative affect, pain and cognitive control in the cingulate cortex. Nat. Rev. Neurosci. 12, 154–167.
Shepherd, J.D., Rumbaugh, G., Wu, J., Chowdhury, S., Plath, N., Kuhl, D., Huganir, R.L., Worley, P.F., 2006. Arc/Arg3.1 mediates homeostatic synaptic scaling of AMPA receptors. Neuron 52, 475–484.
Simpson, J., Kelly, J.P., 2011. The impact of environmental enrichment in laboratory rats–behavioural and neurochemical aspects. Behav. Brain Res. 222, 246–264.
Siuda, D., Wu, Z., Chen, Y., Guo, L., Linke, M., Zechner, U., Xia, N., Reifenberg, G., Kleinert, H., Forstermann, U., et al., 2014. Social isolation-induced epigenetic changes in midbrain of adult mice. J. Physiol. Pharmacol. 65, 247–255.
Snyder-Mackler, N., Burger, J.R., Gaydosh, L., Belsky, D.W., Noppert, G.A., Campos, F.A., Bartolomucci, A., Yang, Y.C., Aiello, A.E., O'Rand, A., et al., 2020. Social determinants of health and survival in humans and other animals. Science 368.
Stankiewicz, A.M., Swiergiel, A.H., Lisowski, P., 2013. Epigenetics of stress adaptations in the brain. Brain Res. Bull. 98, 76–92.
Stillman, B., 2018. Histone modifications: insights into their influence on gene expression. Cell 175, 6–9.
Sun, L., Min, L., Zhou, H., Li, M., Shao, F., Wang, W., 2017. Adolescent social isolation affects schizophrenia-like behavior and astrocyte biomarkers in the PFC of adult rats. Behav. Brain Res. 333, 258–266.
Sun, X., Lin, Y., 2016. Npas4: linking neuronal activity to memory. Trends Neurosci. 39, 264–275.
Suri, D., Veenit, V., Sarkar, A., Thiagarajan, D., Kumar, A., Nestler, E.J., Galande, S., Vaidya, V.A., 2013. Early stress evokes age-dependent biphasic changes in hippocampal neurogenesis, BDNF expression, and cognition. Biol. Psychiatr. 73, 658–666.
Tan, T., Wang, W., Liu, T., Zhong, P., Conrow-Graham, M., Tian, X., Yan, Z., 2021. Neural circuits and activity dynamics underlying sex-specific effects of chronic social isolation stress. Cell Rep. 34, 108874.
Tirelli, E., Laviola, G., Adriani, W., 2003. Ontogenesis of behavioral sensitization and conditioned place preference induced by psychostimulants in laboratory rodents. Neurosci. Biobehav. Rev. 27, 163–178.
Tran, L., Schulkin, J., Ligon, C.O., Greenwood-Van Meerveld, B., 2015. Epigenetic modulation of chronic anxiety and pain by histone deacetylation. Mol. Psychiatr. 20, 1219–1231.
van Praag, H., Kempermann, G., Gage, F.H., 2000. Neural consequences of environmental enrichment. Nat. Rev. Neurosci. 1, 191–198.
van Spronsen, M., Hoogenraad, C.C., 2010. Synapse pathology in psychiatric and neurologic disease. Curr. Neurol. Neurosci. Rep. 10, 207–214.
Vardar, G., Chang, S., Arancillo, M., Wu, Y.J., Trimbuch, T., Rosenmund, C., 2016. Distinct functions of syntaxin-1 in neuronal maintenance, synaptic vesicle docking, and fusion in mouse neurons. J. Neurosci. 36, 7911–7924.
Walf, A.A., Frye, C.A., 2007. The use of the elevated plus maze as an assay of anxiety-related behavior in rodents. Nat. Protoc. 2, 322–328.
Wang, W., Cao, Q., Tan, T., Yang, F., Williams, J.B., Yan, Z., 2021. Epigenetic treatment of behavioral and physiological deficits in a tauopathy mouse model. Aging Cell 20, e13456.
Wang, W., Tan, T., Cao, Q., Zhang, F., Rein, B., Duan, W.M., Yan, Z., 2022a. Histone deacetylase inhibition restores behavioral and synaptic function in a mouse model of 16p11.2 deletion. Int. J. Neuropsychopharmacol. 25, 877–889.
Wang, Z.J., Shwani, T., Liu, J., Zhong, P., Yang, F., Schatz, K., Zhang, F., Pralle, A., Yan, Z., 2022b. Molecular and cellular mechanisms for differential effects of chronic social isolation stress in males and females. Mol. Psychiatr. 27, 3056–3068.
Wang, Z.J., Zhong, P., Ma, K., Seo, J.S., Yang, F., Hu, Z., Zhang, F., Lin, L., Wang, J., Liu, T., et al., 2020. Amelioration of autism-like social deficits by targeting histone methyltransferases EHMT1/2 in Shank3-deficient mice. Mol. Psychiatr. 25, 2517–2533.
Wellman, C.L., Bangasser, D.A., Bollinger, J.L., Coutellier, L., Logrip, M.L., Moench, K. M., Urban, K.R., 2018. Sex differences in risk and resilience: stress effects on the neural substrates of emotion and motivation. J. Neurosci. 38, 9423–9432.
Woodhouse, S.S., Dykas, M.J., Cassidy, J., 2012. Loneliness and peer relations in adolescence. Soc. Dev. 21, 273–293.
Yan, Z., Rein, B., 2022. Mechanisms of synaptic transmission dysregulation in the prefrontal cortex: pathophysiological implications. Mol. Psychiatr. 27, 445–465.
Zelikowsky, M., Hui, M., Karigo, T., Choe, A., Yang, B., Blanco, M.R., Beadle, K., Gradinaru, V., Deverman, B.E., Anderson, D.J., 2018. The neuropeptide Tac2 controls a distributed brain state induced by chronic social isolation stress. Cell 173, 1265–1279 e1219.
Zheng, Y., Liu, A., Wang, Z.J., Cao, Q., Wang, W., Lin, L., Ma, K., Zhang, F., Wei, J., Matas, E., et al., 2019. Inhibition of EHMT1/2 rescues synaptic and cognitive functions for Alzheimer's disease. Brain 142, 787–807.